Optics Letters

Characterization of high-harmonic emission from ZnO up to 11 eV pumped with a Cr:ZnS high-repetition-rate source

Giulio Vampa,[1,*] Sergey Vasilyev,[2] Hanzhe Liu,[1] Mike Mirov,[2] Philip H. Bucksbaum,[1] and David A. Reis[1]

[1]Stanford PULSE Institute, SLAC National Accelerator Laboratory, Menlo Park, California 94025, USA
[2]IPG Photonics—Southeast Technology Center, Birmingham, Alabama 35211, USA
*Corresponding author: gvampa@stanford.edu

Received 26 October 2018; revised 28 November 2018; accepted 30 November 2018; posted 30 November 2018 (Doc. ID 349143); published 4 January 2019

We report the measurement of high-order harmonics from a ZnO crystal with photon energies up to 11 eV generated by a high-repetition-rate femtosecond Cr:ZnS laser operating in the mid-infrared at 2–3 μm, delivering few-cycle pulses with multi-watt average power and multi-megawatt peak power. High-focus intensity is achieved in a single pass through the crystal without a buildup cavity or nanostructued pattern for field enhancement. We measure in excess of 10^8 high-harmonic photons/second.

https://doi.org/10.1364/OL.44.000259

High\-repetition-rate femtosecond (fs) lasers at photon energies of ∼10 eV and beyond are currently in high demand for applications such as time-resolved photoemission [1–3], frequency-comb vacuum-ultraviolet (VUV) spectroscopy [4,5], as well as time-resolved spectroscopy with chemical and elemental specificity.

The prime method to reach this spectral range is by high-order harmonic generation (HHG) driven by ultrafast infrared lasers. The high peak intensity required to generate high harmonics in noble gases, which exceeds 10^{14} W/cm^2, can be achieved at megahertz (MHz) repetition rates if either (i) the gas is placed inside an oscillator cavity [6] or (ii) the oscillator output is coupled to an external buildup cavity that is phase-locked to the oscillator [7,8]. Coherent addition of successive pulses in the train then leads to the required field enhancement; however, the need for stable phase-locked operation of the cavity renders these experiments extremely challenging. Additional limitations imposed by the dispersion of the ionized gas have only been circumvented recently [9]. Intense development of high average power MHz-rate sources has recently enabled extra-cavity high-harmonic generation with a thin-disk oscillator [10], and fs fiber lasers have also been used up to 0.6 MHz [11]. Low harmonics have also been obtained at 10 MHz [12].

An alternative to these schemes has emerged following the demonstration of high-harmonic generation in solids [13], which have generated photon energies of 20–30 eV with focused intensities that are 10–100 times lower than comparable HHG in gases [14–16]. At these reduced intensities, HHG at MHz rates becomes feasible. In an initial demonstration, a conventional Ti:sapphire oscillator with a repetition rate of 75 MHz has been converted to up to 20 eV harmonics in a single pass through sapphire nanocones coated with Au film [17]. A 100-fold enhancement of the peak intensity was obtained at the apex of a tapered cone by means of the metallic coating. More recently, the output of a fs Tm-doped fiber laser has been converted to harmonics up to 4.6 eV in a single pass through Si and ZnO crystals without field enhancement [18]. The authors concluded that a six-fold increase of the peak intensity would have been sufficient to reach 10 eV in ZnO.

Here, we generate high-order harmonics up to 11 eV photon energies in a single pass through a ZnO crystal without field enhancement (Fig. 1). The source is a mid-infrared (MIR) fs high-repetition-rate master oscillator power amplifier (MOPA)

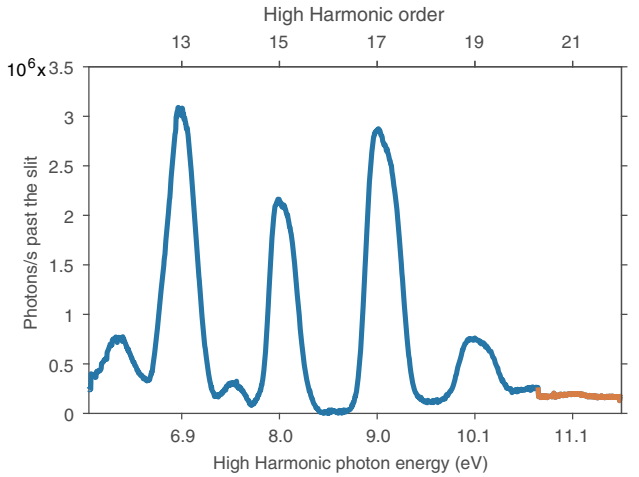

Fig. 1. High-harmonic spectrum generated by our high-repetition-rate Cr^{2+}:ZnS laser system. The high-harmonic spectrum covers the spectral range between ∼6 and ∼12 eV. The yellow spectrum is obtained with a Pt-coated grating.

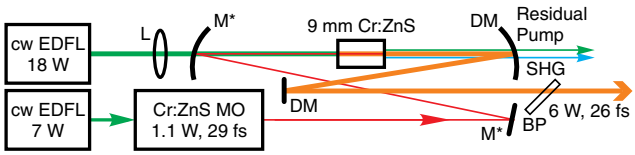

Fig. 2. Few-cycle Cr^{2+}:ZnS MOPA (not to scale): EDFL, pump laser at 1567 nm; MO, Kerr-lens mode-locked Cr:ZnS oscillator; L, pump focusing lens $f = 80$ mm; Cr:ZnS, gain element; $M*$ and BP dispersive mirrors and Brewster plates for dispersion control; SHG signal is generated in the gain element via the RQPM process and separated by dichroic mirrors DM. The setup is enclosed in a dust-tight case that was purged by nitrogen during the spectral measurements.

based on a Cr^{2+}:ZnS gain medium, which delivers three-cycle pulses at a central wavelength of 2.34 μm and a pulse energy of 79 nJ.

The paper is organized as follows. First, we present the capabilities of the laser system employed in this study. Second, we detail the experimental setup for the high-harmonic measurements and report the measured photon flux. Finally, we draw the conclusions.

A MIR fs laser source is arranged as a full-repetition-rate MOPA. It is purpose-built for high-harmonic generation and optimized for short pulse duration. The schematic of the source is illustrated in Fig. 2 with the output parameters in Fig. 3. The design of the generic scheme is described in Ref. [19].

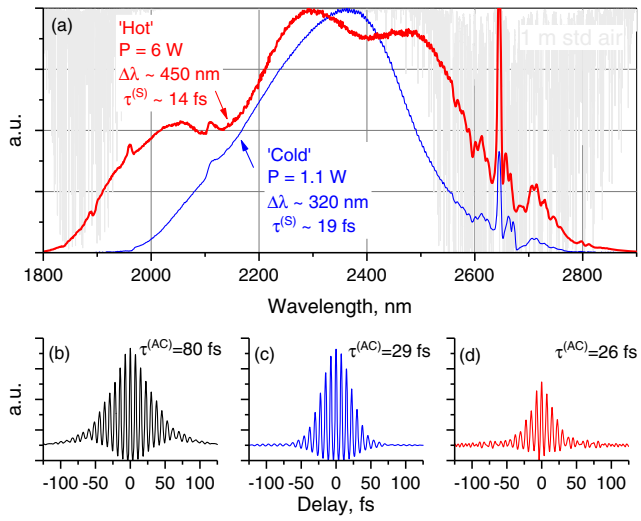

Fig. 3. (a) Measured spectra and (b)–(d) interferometric autocorrelations (IACs) of Cr^{2+}:ZnS MOPA (we used a Princeton Instruments SP2150 monochromator and a custom A·P·E autocorrelator, respectively). Initial spectrum ("cold," amplifier's pump is off) is compared with the final spectrum ("hot," full pump power). Both spectra are normalized to unity. Numbers near the spectra show measured average power (P), spectral bandwidth ($\Delta\lambda$), and transform-limited pulse duration estimated from the spectral bandwidth ($\tau^{(S)}$). Gray background shows transmission of 1 m of air at standard conditions. (b) IAC was acquired behind the OC of the oscillator. (c) and (d) IACs were acquired at the output of the "cold" and "hot" amplifier, respectively. Numbers near the IACs show estimated pulse durations ($sech^2$ fit of the autocorrelation functions). (d) The distortions in the IAC are due to residual second and third harmonic signals. Modified from Ref. [19], to include panel (b).

The plane-parallel cut, AR-coated gain elements are optically pumped by off-the-shelf cw Er-doped fiber lasers (EDFLs) and cooled with room-temperature water. Both the master oscillator and the amplifier are based on polycrystalline Cr^{2+}:ZnS produced in-house. The Cr^{2+}:ZnS oscillator delivers 1.1 W average power at 76.4 MHz pulse repetition frequency (f_R) [20] over a bandwidth of 320 nm [14 THz, FWHM, Fig. 3(a)]. The estimated transform-limited pulse duration is $\tau^{(S)} \approx 19$ fs, assuming the time-bandwidth product is 0.32. The average power for the amplified MIR fs pulses exceeds 6 W, which corresponds to 26% single-pass conversion of low-cost cw EDFL radiation. Nonlinear $\chi^{(3)}$ interactions in the amplifier's gain element [21] result in spectral broadening of the amplified pulses to about 450 nm [23 THz, FWHM, Fig. 3(a)]. A significant fraction of the MIR output is converted to second harmonic via the random quasi-phase-matching (RQPM) process in the polycrystalline gain element. We measure second-harmonic generation (SHG) power in excess of 0.4 W. More details about the spectral broadening of fs seed pulses in the amplifier's gain element are provided in Fig. 27 of Ref. [19].

Few-cycle MIR pulses acquire significant temporal broadening and chirp during their propagation through a 3.2 mm yttrium aluminum garnet (YAG) substrate of the oscillator's output coupler (OC) and the 9-mm-thick Cr^{2+}:ZnS gain element of the amplifier. For instance, presumed $\tau^{(S)} \approx 19$ fs output of the oscillator is broadened to about $\tau^{(AC)} = 80$ fs by the OC with group delay dispersion (GDD) ≈ -480 fs^2 [Fig. 3(b)]. The Cr^{2+}:ZnS gain element has higher dispersion with the opposite sign (GDD $\approx +1120$ fs^2). We use a pair of dispersive mirrors (M^*, GDD ≈ -280 fs^2) for coarse dispersion control, and one 4-mm-thick YAG Brewster plate with negative GDD (-492 fs^2) for fine-tuning of the output pulses. As a result, we measure $\tau^{(AC)} = 29$ fs pulse duration at the output of the "cold" amplifier (i.e., with its pump turned off), as shown in Fig. 3(c). Nonlinear spectral broadening inside the "hot" amplifier results in further reduction of the pulse duration to 26 fs [see Fig. 3(d)]. Thus, we obtain three-cycle pulses at 2.4 μm central wavelength with 79 nJ energy and 2.7 MW peak power at $f_R = 76.4$ MHz.

Measured durations of the re-compressed pulses exceed the limits $\tau^{(S)}$ that can be derived from their spectra, assuming $sech^2$ profiles. This discrepancy is mostly due to significant uncompensated third-order dispersion. The limited dispersion control (over one third of an octave [20,21]) of the available dielectric coatings in the MIR range between 2 and 3 μm currently limit our Cr^{2+}:ZnS oscillators and amplifiers. Recent progress in the technology of MIR coatings will allow us to achieve two-cycle and even sub-two-cycle pulses in the near future. Furthermore, the average power is limited by thermal-optical effects in the gain elements [19]. The recent advent of the spinning ring Cr^{2+}-based lasers and amplifiers has allowed us to mitigate the thermal roll-off and achieve 140 W average power in the cw regime [22] and 27 W power in a 60 fs (eight-cycle) regime [23].

The setup employed to generate high-order harmonics is described below. The output beam of the MOPA is expanded by a telescope composed of a concave mirror ($f = 200$ mm, Au) and a plano-convex lens (CaF_2, $f = 250$ mm, AR coated) and is focused inside a vacuum chamber with a Au-coated 90° off-axis parabola with a nominal $f/\# = 1.2$. The focused beam

passes through a 0.5-mm-thick ZnO single crystal ($11\bar{2}0$) cut. The generated high-harmonic beam is spatially and spectrally analyzed by a VUV spectrometer (McPherson 234) equipped with interchangeable aberration-corrected concave diffraction gratings. An Al-coated grating with 1200 l/mm is suitable for photon energies below 10 eV, while a Pt-coated grating with 2400 l/mm is used for higher photon energies. The diffracted beam is recorded with a Si CCD (Andor, model DO-420-BN). To reduce absorption of the ultraviolet radiation, the chambers are kept at a base pressure of $\sim 1 \times 10^{-2}$ mbar.

To generate high-order harmonics, the focus is positioned towards the exit surface of the crystal, and the laser power is tuned to 2.55 W (~50% of the nominal power) to avoid material damage. The high-harmonic flux is maximized with (i) optimal compression of the pulses in the crystal and (ii) optimal focusing by tuning the separation between the telescope's mirror and lens. This latter procedure minimizes the $f/\#$ while preserving the power transmitted by the optics. The pulse duration is optimized by replacing the 4-mm-thick YAG plate (GDD = −492 fs^2) with a 4-mm-thick CaF_2 plate, bringing the total GDD of the setup to −522 fs^2 (+6%). The peak intensity in vacuum is calculated from the measured input power, the shortest pulse duration of the laser system [26 fs, Fig. 3(d)], and the focus size ($w_0 = 6.7$ μm1/e^2 radius). The focus waist is measured with an objective lens [Mitutoyo Plan APO NIR infinity corrected, NA = 0.42] and a piezo-electric line array (Pyreos), and the finite resolution of the objective (1.7 μm) is deconvoluted. The estimated peak intensity in vacuum is $\sim 1 \times 10^{12}$ W/cm^2. Although incubation at MHz repetition rates may cause thermal melting once the optical breakdown threshold is exceeded [24], the reason for ZnO damage has not been investigated here and is generally not well understood yet.

Figure 1 presents the high-harmonic spectrum covering the range between the 13th harmonic (6.9 eV) and the 21st (11 eV). The measured spectrum greatly extends the energy range covered by high-repetition-rate high-harmonic sources based on a simple single pass and without additional field enhancement [18]. Weak even-order harmonics are also measured. They likely arise from contamination of the driving field with its second harmonic [Fig. 3(d)], which breaks the odd symmetry between maxima and minima of the driving field. The divergence half-angle of the 19th harmonic is 18 mrad, as measured from the spatially

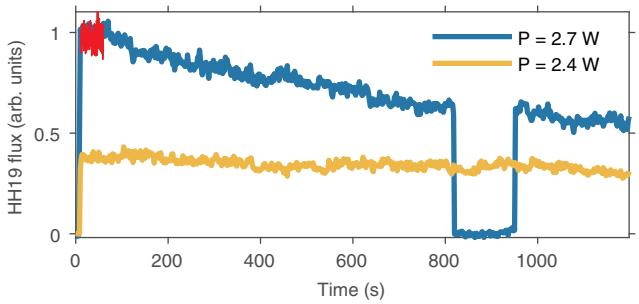

Fig. 4. Flux of the 19th harmonic as a function of time for two input powers (blue and yellow lines). A fresh spot on the crystal is illuminated at the beginning of each temporal sequence. The laser is blocked between 800 and 900 s for the blue trace. The lack of recovery of the high-harmonic power indicates permanent damage to the crystal. The red line shows a fast measurement (10 Hz, 50 ms integration time) with 4% RMS noise.

Table 1. Photon Flux and High-Harmonic Emission Efficiency

	HH15	HH17	HH19
Flux after slit (phot/sec)	1.3×10^8	1.6×10^8	0.4×10^8
Flux at crystal (phot/sec)	6.1×10^8	7.8×10^8	1.8×10^8
Generation efficiency	2×10^{-11}	3×10^{-11}	6×10^{-12}

resolved spectrum (not shown). Figure 4 shows that the photon flux of the 19th harmonic decays to ~70% over 20 min at the highest infrared power, but is stable at ~40% for a slightly lower input power. The fast jitter measured at 10 Hz is about 4% root mean square (RMS, red line). Up to this frequency, neither transient buildup nor decay of the high-harmonic flux have been observed, in contrast to Ref. [18].

Table 1 reports the spectrally and spatially integrated high-harmonic photon flux. The photon flux is calculated from the CCD digital readout (ADU) as

$$S(\omega) = \frac{\text{ADU} \times s}{g \times \text{QE} \times [E_{\text{HH}}(\omega)/3.65] \times \text{exposure}}, \quad (1)$$

where $s = 16.7e/\text{ADU}$ is the sensitivity (factory calibrated), $g = 1$ is the gain, QE = 0.15 is the quantum efficiency (also factory calibrated), taken here to be wavelength-independent over the photon energies detected, E_{HH} is the high-harmonic photon energy, $E_{\text{HH}}/3.65$ counts how many electrons are generated per incident photon, and *exposure* is the exposure time (in seconds).

About 4×10^7 photons/s are measured at the 19th harmonic at 10 eV photon energy. The photon flux at the crystal is estimated by normalizing it to the transmission of the input slit. Assuming a stigmatic high-harmonic beam, the transmission of the slit is $T = P_x^{\text{out}}/P_x^{\text{in}} = P_x/P_y$, where P_x is the power of a given harmonic integrated along the horizontal axis (frequencies), and P_y is that integrated along the vertical axis (beam divergence). In this case, $T = 21\%$, which yields a photon flux in excess of 10^8 photons/sec.

Table 1 also reports the high-harmonic emission efficiency, defined as the ratio between the photon flux at the harmonic wavelength and that at the fundamental (~10^{19} phot/sec). Efficiencies on the order of 10^{-11} are measured for the generation of high harmonics in a ZnO crystal, driven by a MIR laser at 2.34 μm central wavelength at an intensity close to the damage threshold. This efficiency is much smaller than that typical of gas-phase experiments (from ~10^{-6} to 10^{-5}). Part of this difference is attributed to the 100-fold lower intensity used in ZnO, which is further reduced inside the crystal, the longer driving wavelength, and re-absorption of the harmonics by the crystal itself. The efficiency also seems much smaller than that of bulk SiO_2 [15] and MgO crystals, whose flux has been determined to be comparable to that of gases (although an exact quantitative analysis is still lacking). Here too, however, the driving intensity is ~10 times higher than in ZnO, and the driving wavelength is shorter. Reported emission efficiencies at 5.5 eV from ZnO driven with a 50 kHz source, eight-cycle pulses centered at 3.8 μm wavelength are also much higher (10^{-7}) [25]. The reason for the lower efficiency remains to be determined. With looser focusing and kilohertz (kHz) repetition rates, the harmonic emission efficiency from 100 s μm-thick MgO is only mildly affected by spatio-temporal self-action effects on the intense infrared

driver [26]. By analogy, crystal thickness in this experiment should not significantly affect the emission efficiency. Furthermore, in our experience, tight focusing towards the exit surface helps mitigate propagation effects.

In conclusion, we have demonstrated solid-state HHG into the VUV at 76 MHz repetition rate using a Cr^{2+}:ZnS MOPA. The long MIR wavelength is suitable for the excitation of low to wide bandgap materials with high field strength, without incurring deleterious few-photon absorption and the ensuing decrease of the damage threshold. The relatively high pulse energy enables the conversion of MIR light to short-wavelength radiation in a simple single pass through the crystal, without field enhancement provided by nanopatterned surfaces or buildup cavities. Moreover, we have characterized the high-harmonic photon flux from a ZnO crystal to be $\sim 10^8$ photons/sec/harmonic and extracted a conversion efficiency of about 10^{-11} per harmonic, which is orders of magnitude lower than typical gas-phase experiments. Our measurements are a testbed for theoretical work aimed at a quantitative analysis of ionization rates and high-harmonic emission efficiency in solids. Our demonstration of high-repetition-rate high harmonics eases the investigation of strong-field phenomena in nanoscale and low-dimensional solids, where the detected photon flux is limited by the small emission volume.

Progress in thermal dissipation and in MIR dispersive dielectric coatings [27] promise to reach intensities beyond the 10 TW/cm^2 level, thereby enabling excitation of wider bandgap materials such as MgO and SiO_2, where generation of 20–30 eV high harmonics has been demonstrated only with low-repetition-rate amplified laser systems. We foresee that Cr^{2+}-doped high-power lasers will become the workhorse of strong-field science in solids in the near future, taking the stage that once belonged to Ti:sapphire amplified systems.

Finally, the high high-harmonic photon energy is useful for frequency-comb spectroscopy with greater precision than currently possible. For applications to comb spectroscopy, we calculate that the photon flux in each tooth of the comb is $\gtrsim 700$ photons/sec/tooth at the 17th harmonic.

Funding. W. M. Keck Foundation.

Acknowledgment. This work is supported by the W. M. Keck Foundation and Stanford University. The authors thank the Stanford Photonic Research Center and IPG Photonics for equipment gifts and R. Coffee for equipment loans.

REFERENCES

1. A. K. Mills, S. Zhdanovich, F. Boschini, M. Na, M. Schneider, P. Dosanjh, D. Wong, G. Levy, A. Damascelli, and D. J. Jones, in *CLEO: Science and Innovations* (Optical Society of America, 2017), p. STu1I–2.
2. C. Corder, P. Zhao, X. Li, M. D. Kershis, M. G. White, and T. K. Allison, Proc. SPIE **10519**, 105190B (2018).
3. P. Miotti, F. Cilento, R. Cucini, A. De Luisa, A. Fondacaro, F. Frassetto, D. Kopi, D. Payne, A. Sterzi, T. Pincelli, G. Panaccione, F. Parmigiani, G. Rossi, and L. Poletto, in *Compact EUV & X-ray Light Sources* (Optical Society of America, 2018), p. EW2B–5.
4. R. T. Zinkstok, S. Witte, W. Ubachs, W. Hogervorst, and K. S. Eikema, Phys. Rev. A **73**, 061801 (2006).
5. A. Cingöz, D. C. Yost, T. K. Allison, A. Ruehl, M. E. Fermann, I. Hartl, and J. Ye, Nature **482**, 68 (2012).
6. F. Labaye, M. Gaponenko, V. J. Wittwer, A. Diebold, C. Paradis, N. Modsching, L. Merceron, F. Emaury, I. J. Graumann, C. R. Phillips, C. J. Saraceno, C. Kränkel, U. Keller, and T. Südmeyer, Opt. Lett. **42**, 5170 (2017).
7. I. Pupeza, S. Holzberger, T. Eidam, H. Carstens, D. Esser, J. Weitenberg, P. Rußbüldt, J. Rauschenberger, J. Limpert, T. Udem, A. Tünnermann, T. W. Hänsch, A. Apolonski, F. Krausz, and E. Fill, Nat. Photonics **7**, 608 (2013).
8. A. K. Mills, T. Hammond, M. H. Lam, and D. J. Jones, J. Phys. B **45**, 142001 (2012).
9. G. Porat, C. M. Heyl, S. B. Schoun, C. Benko, N. Dörre, K. L. Corwin, and J. Ye, Nat. Photonics **12**, 387 (2018).
10. F. Emaury, A. Diebold, C. J. Saraceno, and U. Keller, Optica **2**, 980 (2015).
11. S. Hädrich, A. Klenke, J. Rothhardt, M. Krebs, A. Hoffmann, O. Pronin, V. Pervak, J. Limpert, and A. Tünnermann, Nat. Photonics **8**, 779 (2014).
12. P. Storz, J. Tauch, M. Wunram, A. Leitenstorfer, and D. Brida, Laser Photon. Rev. **11**, 1700062 (2017).
13. S. Ghimire, A. D. DiChiara, E. Sistrunk, P. Agostini, L. F. DiMauro, and D. A. Reis, Nat. Phys. **7**, 138 (2011).
14. Y. S. You, D. A. Reis, and S. Ghimire, Nat. Phys. **13**, 345 (2017).
15. T. T. Luu, M. Garg, S. Y. Kruchinin, A. Moulet, M. T. Hassan, and E. Goulielmakis, Nature **521**, 498 (2015).
16. G. Ndabashimiye, S. Ghimire, M. Wu, D. A. Browne, K. J. Schafer, M. B. Gaarde, and D. A. Reis, Nature **534**, 520 (2016).
17. S. Han, H. Kim, Y. W. Kim, Y.-J. Kim, S. Kim, I.-Y. Park, and S.-W. Kim, Nat. Commun. **7**, 13105 (2016).
18. K. F. Lee, X. Ding, T. Hammond, M. Fermann, G. Vampa, and P. Corkum, Opt. Lett. **42**, 1113 (2017).
19. S. B. Mirov, I. S. Moskalev, S. Vasilyev, V. Smolski, V. V. Fedorov, D. Martyshkin, J. Peppers, M. Mirov, A. Dergachev, and V. Gapontsev, IEEE J. Sel. Top. Quantum Electron. **24**, 1 (2018).
20. S. Vasilyev, I. Moskalev, M. Mirov, S. Mirov, and V. Gapontsev, Opt. Lett. **40**, 5054 (2015).
21. S. Vasilyev, I. Moskalev, M. Mirov, V. Smolski, S. Mirov, and V. Gapontsev, Opt. Mater. Express **7**, 2636 (2017).
22. I. Moskalev, S. Mirov, M. Mirov, S. Vasilyev, V. Smolski, A. Zakrevskiy, and V. Gapontsev, Opt. Express **24**, 21090 (2016).
23. S. Vasilyev, I. Moskalev, V. Smolski, J. Peppers, M. Mirov, S. Mirov, and V. Gapontsev, *Adv. Solid State Lasers Conference* (2018), p. AW3A.1.
24. C. B. Schaffer, J. F. Garca, and E. Mazur, Appl. Phys. A **76**, 351 (2003).
25. S. Gholam-Mirzaei, J. Beetar, and M. Chini, Appl. Phys. Lett. **110**, 061101 (2017).
26. G. Vampa, Y. You, H. Liu, S. Ghimire, and D. Reis, Opt. Express **26**, 12210 (2018).
27. V. Pervak, T. Amotchkina, Q. Wang, O. Pronin, K. Mak, and M. Trubetskov, *Adv. Solid State Lasers Conference* (2018), p. AW3A.2.